International Journal of Heat and Fluid Flow 74 (2018) 53–64

Contents lists available at ScienceDirect

International Journal of Heat and Fluid Flow

journal homepage: www.elsevier.com/locate/ijhff

Axisymmetric jet impingement on a dimpled surface: Effect of impingement location on flow field characteristics

R. van Hout[*,a], V. Rinsky[a], N. Sasson[c], C. Hershcovich[b], M. Tshuva[c], Y.J. Grobman[b]

[a] The Faculty of Mechanical Engineering, Technion Israel Institute of Technology, Technion city, Haifa, Israel
[b] The Faculty of Architecture and Town planning, Technion Israel Institute of Technology, Technion city, Haifa, Israel
[c] Afeka Academic College of Engineering, Tel-Aviv, Israel

ARTICLE INFO

Keywords:
Impinging jet
Dimpled surfaces
Primary-secondary vortex interaction
Self-similarity
Particle Image Velocimetry

ABSTRACT

Few studies have investigated the flow characteristics of jets impinging on dimpled surfaces that may increase or decrease their heat transfer capabilities. Here, particle image velocimetry (PIV) measurements have been performed on a round jet (diameter D) impinging on a surface having large spherical dimples (opening size d), $D/d = 0.83$. In particular, the effect of jet impingement location on the flow field was investigated. Impingement of the jet centered on the "dimple" as well as on the flat surface between the dimples ("isthmus"), was compared to impingement on a smooth surface. Measurements were performed at three Reynolds numbers, $\langle Re \rangle$ = 1,352, 6,268 and 12,342 at a stand-off distance of $4.8D$. Results showed that the flow field in the developing wall jet strongly changed for "isthmus" impingement while for "dimple" and "smooth" impingement it was similar. However, outer-layer self-similarity was not attained in the developing wall jet. Furthermore, secondary vortex generation as a result of primary vortex impingement, was the same for "smooth" and "dimple" impingement while for "isthmus" impingement, secondary vortices were created through the generation of an unsteady separation bubble.

1. Introduction

The published research on jets impinging on surfaces that are flat or have concavities (Lee et al., 1999) is extensive as impinging jets are known for their high heat transfer coefficients that are affected by many parameters such as turbulence level, jet confinement, nozzle shape and stand-off distance, amongst others (Yule, 1978; Geers et al., 2004; Knowles and Myszko, 1998; Krishnan and Mohseni, 2010; Banyassady and Piomelli, 2015; Zuckerman and Lior, 2007). Many investigations have been performed on jets impinging on flat surfaces (Cooper et al., 1993; Nishino et al., 1996; Fairweather and Hargrave, 2002; Hall and Ewing, 2006; Hadžiabdić and Hanjalić, 2008; Shademan et al., 2016) set at different stand-off distances, H (see Fig. 1), and at a variety of Reynolds numbers, $\mathrm{Re} = U_j D/\nu$, where U_j is the jet exit velocity, D the jet nozzle diameter, and ν is the fluid kinematic viscosity. In jet impingement, typically three regions can be distinguished: (i) the free jet (Yule, 1978), (ii) the stagnation or impingement region (Geers et al., 2004) and (iii) the radially expanding wall jet (Knowles and Myszko, 1998; Krishnan and Mohseni, 2010; Banyassady and Piomelli, 2015). Each of these regions is characterized by different turbulence mechanisms making it difficult to perform accurate numerical simulations (Zuckerman and Lior, 2007).

The mechanism thought to be responsible for the high heat and mass transfer coefficients obtained by impinging jets is the interaction between primary and secondary vortices. The former are generated in the shear layer of the free jet as a result of Kelvin-Helmholtz instabilities and prior to break-up represent toroidal vortices encircling the jet's perimeter (Violato et al., 2012). The latter are generated by the action of the primary vortices upon impingement on the target surface. After impingement, the developing wall jet is characterized by partially overlapping inner and outer shear layers. It is thought that the latter is governed by the incoming turbulence of the free jet while the former develops close to the wall. The wall-normal position, z_m, of maximum radial velocity, U_m, represents an inner-layer scale while the wall jet's half width, $z_{1/2}$, defined as the position farthest away from the wall where the radial velocity equals $0.5U_m$, represents an outer layer scale.

In recent years, with the advent of advanced 3D surface designs and printing techniques, different wall morphologies, such as protrusions or indentations (dimples) that may enhance or reduce heat transfer have become of interest (Grobman and Elimelech, 2016; Hershcovich et al., 2017). However, relatively little is known about the effect of surfaces having "large" dimples ($D/d < 1$, where d is the dimple opening size;

* Corresponding author. Tel.: +(972)-4-8293866.
E-mail address: rene@technion.ac.il (R.v. Hout).

https://doi.org/10.1016/j.ijheatfluidflow.2018.09.010
Received 1 July 2018; Received in revised form 12 September 2018; Accepted 17 September 2018

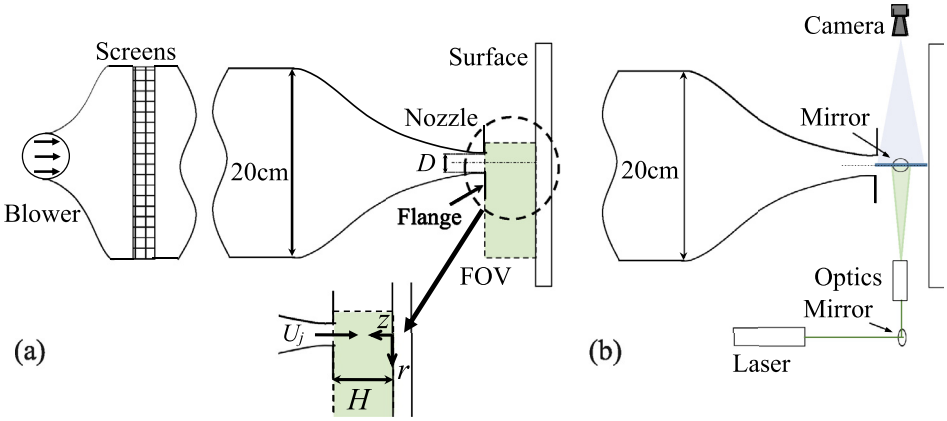

Fig. 1. Schematic layout of the experimental setup (Not to scale). (a) Side view, (b) Top view of PIV setup.

dimple depth is denoted by δ) on the flow field and heat transfer characteristics. Here, in contrast to the study by van Hout et al. (2018b) we focus on jet impingement on dimpled surfaces for which the dimple diameter is larger than the jet's nozzle diameter, $D/d < 1$. While there have been studies on jet impingement onto dimpled surfaces (Ortega-Casanova and Granados-Ortiz, 2014; Azad et al., 2000; Ekkad and Kontrovitz, 2002; Kanokjaruvijit and Martinez-Botas, 2010), few have studied the case where $D/d < 1$. Exceptions are the jet impingement studies onto a single dimple by a few researchers (Terekhov et al., 2006; 2009; Terekhov and Kalinina, 2011; Xie et al., 2013; Hashiehbaf et al., 2015) who concluded that depending on the ratios of D/d and δ/d, both heat transfer enhancement as well as suppression can be obtained. Xie et al. (2013) and Terekhov et al. (2009) found that for a deep dimple, $\delta/D \geq 0.26$, a large scale, pulsating toroidal vortex formed inside the dimple resulting in decreased local Nusselt numbers. However, the increased total heat transfer area due to the dimples resulted in overall higher heat transfer when $D/d \leq 0.5$. In contrast, when $D/d = 1.045$, the opposite was observed. Both Xie et al. (2013) and Terekhov et al. (2009) showed that for a shallow dimple, $\delta/D \leq 0.13$ and $D/d = 0.19$, the flow field characteristics were similar as for impingement on a smooth surface.

Besides the experimental study by van Hout et al. (2018b) and the numerical simulations by Ortega-Casanova and Granados-Ortiz (2014), a single round jet impinging on a dimpled surface and in particular the development of the radial wall jet has not been studied. Both studied the case where $D/d \geq 2$. The results by Ortega-Casanova and Granados-Ortiz (2014) indicated that at the stagnation point, heat transfer can be enhanced or at least be as good as the flat plate case regardless of stand-off distance and if the jet included swirl or not. Furthermore, in most cases dimpled surfaces enhanced global heat transfer. van Hout et al. (2018b) focused on the flow field characteristics and showed that despite significantly changed surface morphology as a result of the dimples, the flow field in the radial developing wall jet attained outer layer self-similarity. In addition, the generation and evolution of the secondary vortices resulting from impingement of primary vortices was the same as for smooth plate impingement. To the best of the authors' knowledge, there are no published measurements of the heat transfer nor flow field characteristics of a single round jet impinging on a dimpled surface when $D/d < 1$.

The goal of the present study is to measure the flow field of a single round jet impinging on a dimpled surface characterized by $D/d = 0.83$ and $\delta/d = 0.77$. In particular, the effect of the impingement location, i.e. centered on the "dimple" or on the flat surface ("isthmus") between the dimples, will be studied using particle image velocimetry (PIV). This research is a continuation of that reported by van Hout et al. (2018b) who studied jet impingement on dimpled plates with $D/d > 2$ using the same facility. The experimental setup and data processing are described in Section 2 while the results are presented in Section 3. A summary and conclusions are given in Section 4.

2. Experimental setup and data processing

The round jet was issued from a contraction attached to the exit of a windtunnel test section (van Hout et al., 2018a) that smoothly changed from a square cross-section (20×20 cm^2) to a round circular jet ($D = 20$ mm, contraction area ratio of 100:1, Fig. 1). The air jet impinged on a vertically placed gypsum surface (20×20 cm^2) at a stand-off distance, $H/D = 4.8$. Besides a smooth target surface, a dimpled target surface was designed and 3D printed (Table 1). The dimples were spherically shaped and had a dimple opening size, $d = 24$ mm ($D/d = 0.83$). The ratio between the dimple depth and opening size, δ/d, equaled 0.77 (Table 1). The jet impinged in three different ways onto the surfaces: (i) impingement on the "smooth" target surface, acting as the baseline measurement; (ii) impingement centered at the dimple center ("dimple", Table 1) and (iii) impingement centered on the flat surface area in between the dimples ("isthmus", Table 1).

Experiments were performed at three mean jet exit velocities, $\langle U_j \rangle = 1.08 \pm 0.08, 5.00 \pm 0.01$ and 9.84 ± 0.03 m/s corresponding to mean, jet Reynolds numbers of $\langle \mathrm{Re} \rangle = 1{,}351 \pm 100, 6{,}268 \pm 19$ and $12{,}342 \pm 28$. Actual experimental conditions for each impingement condition are summarized in Table 1. A schematic system layout including the right-handed cylindrical coordinate system is depicted in Fig. 1, where r, z denote the radial and axial directions, respectively; θ (not shown) denotes the azimuthal direction. Corresponding instantaneous velocities are denoted by U_r, U_θ and U_z and fluctuating (Reynolds decomposed) velocities by u_r, u_θ and u_z; Angle brackets, $\langle .. \rangle$, denote ensemble averaged values and a prime " ′ " denotes the root-mean-square (rms) value. Bold typeface denotes vectors.

The flow field was measured using a PIV system comprising a CCD camera (2048×2048, 7.4×7.4 μm^2 pixels), an Nd:Yag laser (Litron lasers, Nano-L, 200 mJ/pulse at 15 Hz), laser sheet optics and data acquisition/processing software (DaVis 8.1, LaVision GmbH). The laser sheet (1 mm thick) vertically crossed the jet's centerline (Fig. 1b) and was aligned with the centers of an array of dimples (see Table 1). The camera's field of view (FOV) was 100×130 mm^2, covering the jet, the impingement region and part of the radially expanding wall jet. The flow field inside the dimples was not measured due to lack of optical access. Tracer particles (0.2-0.3 μm diameters, glycerine BP/purified water mixture "Smoke Fluid A", Concept Engineering Limited) were generated by a portable smoke generator (Colt 4) and introduced at the blower's entrance to ensure a spatially uniform distribution at the nozzle exit. At each Re and for each impingement condition, five data sets were acquired at an acquisition rate of 7 Hz, totaling 450 statistically independent pairs of PIV images. These were processed using a multi-pass algorithm based on the fast Fourier transform (FFT, DaVis 8.1) starting with an interrogation window size of 64×64 pixels that